A Linear Analysis for the Flight Path Control of the Cassini Grand Finale Orbits

By Mar VAQUERO,[1)] Yungsun HAHN,[1)] Duane ROTH,[1)] and Mau WONG[1)]

[1)] *Jet Propulsion Laboratory / California Institute of Technology, Pasadena, CA*

(Received June 21st, 2017)

Cassini's Grand Finale Mission begins after the last targeted Titan flyby on April 22, 2017 and ends with a series of 22 ballistic orbits each passing within a few thousand kilometers of the cloud tops of Saturn, ultimately impacting the planet on September 15, 2017. Despite the ballistic nature of the trajectory, the absence of targeted maneuvers throughout the final orbits causes position uncertainties to grow exponentially with time, posing a significant difficulty for the science sequence planning team. Thus, a strategy that incorporates trajectory correction maneuvers was developed to significantly reduce dispersions from the reference path and maintain dispersions below 250 km (1-σ). In this paper, the linear method used to determine the optimal number and location of the maneuvers to control the trajectory, along with the corresponding targets, is detailed. A nonlinear Monte Carlo trajectory dispersion tool served as a testbed to validate the linear analysis results. Based on orbit determination covariance sampling with Monte Carlo simulations, the linear approach allowed the Cassini maneuver analysts to run thousands of maneuver combinations in little time, eventually finding an optimal strategy with three statistical maneuvers ($\Delta V99 < 1.5$ m/s) to adequately control most of the trajectory.

Key Words: Cassini, Linear Analysis, Covariance Sampling, Monte Carlo Simulation

Nomenclature

Subscripts	0	:	initial
	f	:	final
	p	:	perturbed
	INT	:	integrated
	STM	:	State Transition Matrix
	OTM	:	Orbit Trim Maneuver
Acronyms	OD	:	Orbit Determination
	RCS	:	Reaction Control System
	SVD	:	Singular Value Decomposition
	P	:	Periapsis

1. Introduction to The Problem

After almost twenty years of successful mission operations and invaluable scientific discoveries, the Cassini orbiter continues to tour Saturn on the most complex gravity-assist trajectory ever flown.[1–3)] The mission is soon coming to an end with a series of 22 highly inclined (62 degrees), short period (6.5 days), ballistic orbits each passing within a few thousand kilometers of the cloud tops of Saturn. On September 15, 2017, the spacecraft will dive into Saturn's atmosphere and become permanently captured. The end of mission trajectory depicted in Fig. 1 was incorporated in the final phase of the Solstice Mission after multiple studies were carried out to ensure that, per Planetary Protection requirements and before the spacecraft runs out of propellant, the possibility of future impact with any of the large icy moons, such as Enceladus, was precluded.[4)]

The Cassini science sequence planning team expects to receive high volumes of unique science data from various onboard instruments throughout the Grand Finale Mission. This data return is vastly improved if pointing and timing errors are reduced such that key observations can be identified and located with high precision. However, the absence of targeted maneuvers throughout the 22 final ballistic orbits causes position uncertainties to grow exponentially with time, posing a significant difficulty for the sequence planning team. Thus, it was of great interest to develop a strategy that incorporates trajectory correction maneuvers to significantly reduce dispersions from the reference path, eliminating late sequence updates and facilitating sequence planning tasks. Although controlling the trajectory to reduce position uncertainties is highly desirable, Saturn atmospheric entry on September 15, 2017 must be guaranteed, as detailed by the following set of end of mission requirements:

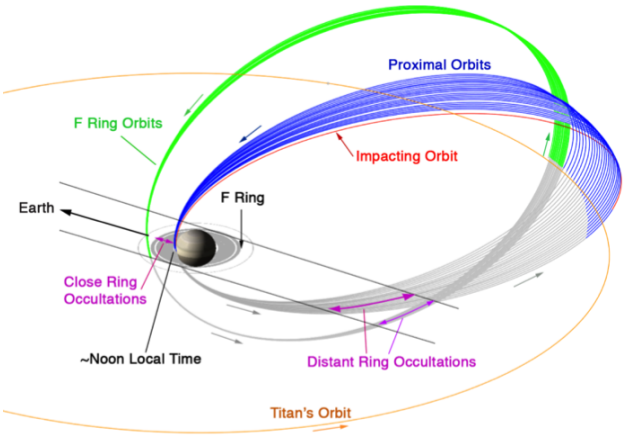

Fig. 1. Representation of Cassini's Grand Finale trajectory encompassing the F-ring orbits (green), the Grand Finale orbits (blue), and the final orbit (red) culminating with Saturn atmospheric entry on September 15, 2017.

- Achieve Saturn atmospheric entry at end of mission (radius $< 60,848$ km).
- Ensure that the spacecraft is safe from ring particle impact at the descending ring plane crossing (radius $\leq 64,300$ km to avoid D-ring dust and entering the outer F-ring boundary).
- Ensure that the spacecraft is above tumble density at Saturn periapsis (radius $> 61,750$ km).

The trajectory control requirements to maintain the spacecraft in the "safe" zone during the final 22 orbits are summarized in Fig. 2. To meet these requirements, the Cassini Navi-

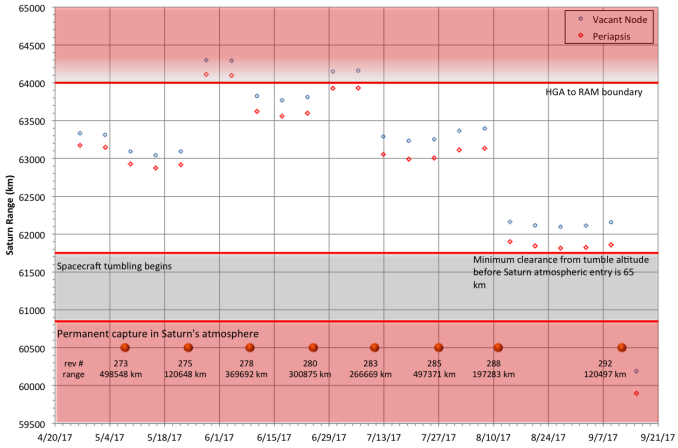

Fig. 2. Schematic of Cassini's end of mission 'safe" corridor: the red dots represent each of the 22 periapses locations and the solid red lines mark the three safety boundaries: HGA to RAM to protect the instruments from any dust particles, clearance from tumbling altitude, and permanent capture into Saturn's atmosphere.

gation Team faces a targeting paradigm shift, i.e., the goal becomes staying as close as possible to the reference trajectory overall instead of focusing on meeting a flyby target accuracy. Along this set of requirements, a number of science requests are also detailed:

- Remain – overall – within 250 km (68% probability) of the reference trajectory.
- Provide trajectory dispersion plots to assist with science planning activities.
- Specify the number and locations of impulsive maneuvers to reserve time within the sequence from other activities.
- Avoid scheduling maneuvers during occultations or within ±12 hours of Saturn periapsis.
- Limit the number of maneuvers to allow maximum time for science data collection.

An added difficulty in the design of a suitable trajectory control strategy is presented by the amount of propellant left in the tanks to maneuver the spacecraft. As of February 22, 2017 (completion of OTM468A), about 27 m/s of usable ΔV propellant is estimated to be available for maneuvers at the end of mission (at the 90th percentile), which accounts for approximately 1.1% of the mission total. With such constrained propellant margin, the exploration of different maneuver strategies for preserving propellant becomes a driving factor in the design process.

Determining the optimal number and location of the maneuvers to control the trajectory, along with the corresponding targets, was a nontrivial task. Several strategies were attempted until a feasible solution was found via two different approaches: a linear analysis to strategize maneuver and target placement and a nonlinear analysis to produce final trajectory dispersions. Both methods are based on orbit determination covariance sampling with Monte Carlo simulations. The linear method maps uncertainties from a given state to a future time while the nonlinear approach is based on numerical state integration. After cautious initial testing, it was determined that the results from both methods were in agreement with insignificant differences, allowing the maneuver analysts to confidently run thousands of maneuver combinations in little time. The control strategy ultimately adopted by the Cassini Project and the trajectory dispersion results from the nonlinear approach were detailed in a paper by Wong et. al.[5] In this paper, the results from the linear Monte Carlo approach are detailed along with the different strategies that led to a ΔV-optimal solution to control the position uncertainties along the proximal orbits, highlighting the benefits of adopting a linear technique for preliminary studies.

2. Solution Approach

Unlike the primary mission, where maneuvers were designed to precisely target the desired satellite flyby conditions, the control strategy during the proximal mission is to "stay close" (within 250 km, 1-σ) to the reference trajectory while minimizing the number of maneuvers and the total ΔV. To solve the problem, members of the Cassini Navigation Team examined the trades and carried out analyses used to develop the maneuver strategy for controlling the trajectory during the proximal mission, focusing on two tasks: number and location of maneuvers and location of targets.

2.1. Validating the Linearity of the Trajectory

To proceed confidently with the proposed linear approach, the linearity of the trajectory needs to be validated. There are many different ways to do so, but in this analysis a simple and straightforward perturbation/propagation approach was used, where the reference trajectory is initially ($\mathbf{X}_0(t_0)$) perturbed by a certain amount ($\Delta\mathbf{X}_0$) and propagated forward to an end time (t_f). The final state associated with the perturbed trajectory, $\mathbf{X}_p(t_f)$, is then compared to the final state of the reference trajectory ($\mathbf{X}_f(t_f)$). The deviation from the truth at t_f is then estimated two ways: via the state transition matrix (STM) and by computing the difference between the numerically (nonlinear) integrated states, as depicted in Fig. 3.

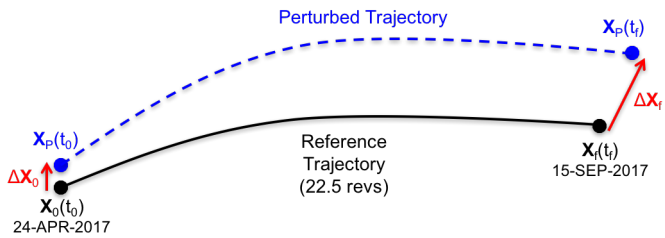

Fig. 3. A simple way of assessing the linearity of the reference trajectory.

The eigenvalues (λ_i) and eigenvectors ($\mathbf{v}_i$) from the initial orbit determination (OD) covariance matrix are then used to estimate the size of the initial perturbation, $\Delta\mathbf{X}_0$, via singular value decomposition (SVD),

$$SVD = \sum_{i=1,6} n_i \lambda_i \mathbf{v}_i \tag{1}$$

resulting in six perturbed initial states in the direction of each

eigenvector (n_i = 1 for 1-σ perturbation), given by:

$$
\begin{aligned}
\mathbf{X}_{p1} &= \mathbf{X}_0 + \lambda_1 \mathbf{v}_1 \\
\mathbf{X}_{p2} &= \mathbf{X}_0 + \lambda_2 \mathbf{v}_2 \\
\mathbf{X}_{p3} &= \mathbf{X}_0 + \lambda_3 \mathbf{v}_3 \\
\mathbf{X}_{p4} &= \mathbf{X}_0 + \lambda_4 \mathbf{v}_4 \\
\mathbf{X}_{p5} &= \mathbf{X}_0 + \lambda_5 \mathbf{v}_5 \\
\mathbf{X}_{p6} &= \mathbf{X}_0 + \lambda_6 \mathbf{v}_6
\end{aligned}
\tag{2}
$$

with the largest perturbation being 82 km in position and 15 cm/s in velocity. Once the vector difference, $\|\Delta\mathbf{X}_{f(INT)} - \Delta\mathbf{X}_{f(STM)}\|$, is calculated, its magnitude is plotted as a function of time for each time interval from t_0 to t_f. For illustration purposes, the worst case corresponding to $\mathbf{X}_{p2}$ is plotted in Fig. 4. The peaks on the graph correspond to periapsis locations.

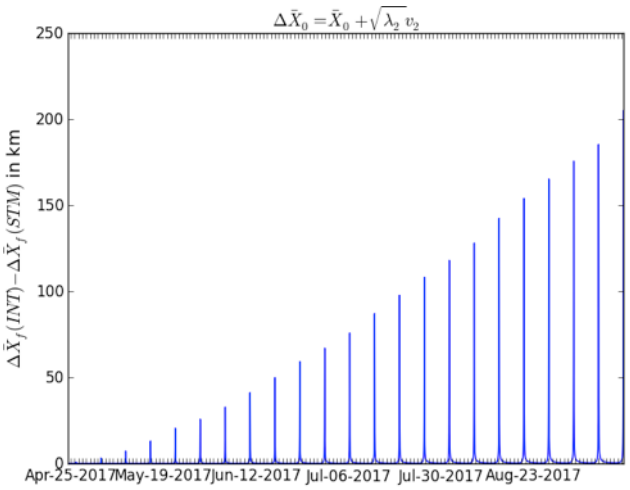

Fig. 4. Integration vs. STM mapping: $\Delta\mathbf{X}_f$ vector difference in km as a function of time for the worst case scenario corresponding to $\mathbf{X}_{p2}$ in Eq. 2.

A discrepancy of less than 200 km over 22.5 orbits suggests that the trajectory behaves fairly linearly, indicating that a linear approach is suitable to solve the maneuver design problem.

2.2. The Uncontrolled Trajectory

After performing a detailed OD covariance analysis with simulated Doppler and range tracking data, it was determined that the Titan-126 (T126) flyby error dominates the resulting covariance. The downtrack dispersions are largest by far, with peaks at periapsis and troughs at apoapsis, as illustrated in Fig. 5, indicating that the dispersions are primarily related to orbit period differences. The trajectory dispersion plots in Fig. 5 are generated by filtering simulated tracking data from the arc epoch of April 9, 2017 to the data cutoff for the last control point prior to T126 on 18-April-2017 and then mapping the resulting covariance past T126. Considered errors in the covariance analysis include ephemeris and masses of Saturn and its satellites, Saturn's pole orientation, tracking station locations, Earth's polar motion, and media effects. By the last periapsis, the 7,757 km along-track dispersion is roughly equivalent to a dispersion in periapsis time of 226 seconds. Additionally, the distribution of dispersions approaching and departing periapsis is close to one-dimensional. Even though the uncertainty in radius at the last periapsis is 25 km, Saturn atmospheric capture is statistically guaranteed.

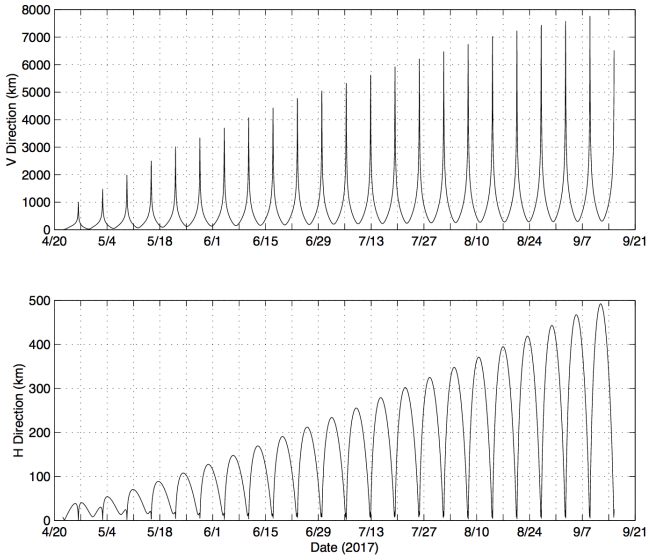

Fig. 5. Uncontrolled (no maneuvers) trajectory dispersion plots in three spatial dimensions based on orbit determination analysis for the uncontrolled trajectory with no maneuvers after OTM469.[5] For reference, V denotes along-track direction and H represents the angular momentum direction.

If left uncontrolled, that is, if no maneuvers are performed after the last approach maneuver (OTM469) before the last targeted flyby (T126), the position dispersions can grow to almost 8000 km, 1-σ, as illustrated in Fig. 5. Recall that the goal is to stay within 250 km (1-σ) from the reference path at all times, if possible, which is never achieved if left uncontrolled. Figure 6 illustrates the overall 68% position dispersion as a function of time resulting from the nonlinear propagation of 1000 sample trajectories, each combining dispersion contributions from the initial T126 flyby, subsequent Reaction Control System (RCS) thruster events, and uncertainties in the atmospheric drag force.

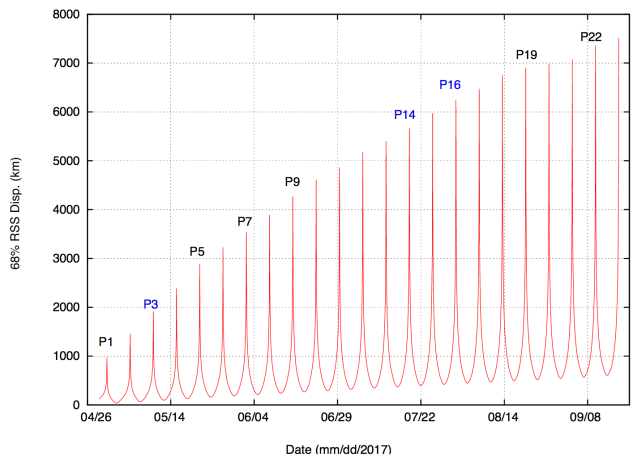

Fig. 6. Overall uncontrolled dispersions for the 22 proximal orbits (periapsis-1 through periapsis-22) resulting from the nonlinear analysis relying on numerical integration. Peaks are locations of periapses[5]

To demonstrate the agreement, to the first order, between the nonlinear and linear models used in this investigation, consider the plot in Fig. 7, which represents the same results based on the linear approach. It is apparent that the along-track (timing)

component in Fig. 6 and Fig. 7 exhibits similar behavior, validating the linear approach adopted to solve this problem.

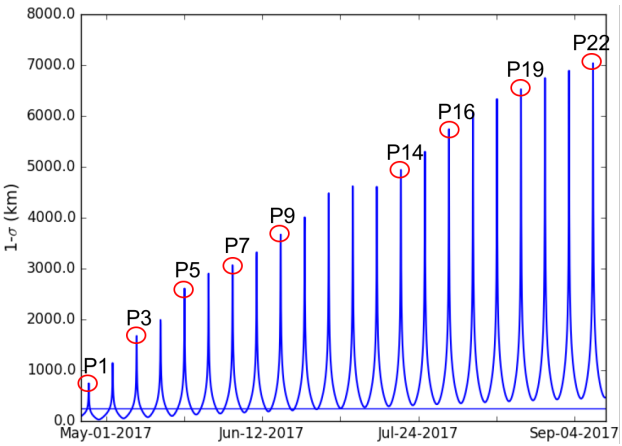

Fig. 7. Overall uncontrolled dispersions for the 22 proximal orbits (periapsis-1 through periapsis-22) resulting from the linear analysis relying on linear mappings. Peaks and troughs correspond to locations of periapsis and apoapsis, respectively, and the solid blue line at the bottom represents the 250 km control threshold.

2.3. Control Strategy for the Cassini Grand Finale

The analysis for strategizing maneuver and target placement is divided into two tasks: 1) determining the periapsis to target to along the entire reference trajectory in order to optimize the trajectory control and reduce the dispersions to a minimum and 2) once a target is selected, determining the optimal location of the targeting maneuver to minimize ΔV cost. Taking advantage of the computational speed of the linear process, the first task is tackled experimentally via a brute force approach in which a large number of simulations are considered and the best trajectory control design is eventually selected. Once the target location is determined, an effective and quick way of calculating the optimal maneuver location to target to the selected periapsis (second task) is to exploit the upper right 3×3 block of the state transition matrix. Because of the computationally expensive aspect of the nonlinear method, an exhaustive, brute force search like this one could not have been carried by numerical integration of thousands of sample trajectories. Of course, the results of the final, optimal strategy obtained via the linear approach is always validated wth a nonlinear, numerical process.

2.3.1. Target Placement Analysis

To reduce the design space as much as possible, a number of constraints are imposed on the problem:

- The location of the first maneuver is fixed on 24-APR-2017 19:15:00 ET (approx. 2 days after T126)
- Maneuvers must not be placed ±1 day from periapsis
- A backup maneuver opportunity must be included, per nominal spacecraft requirements and procedures

Additionally, the number of maneuvers must be limited to avoid interference with science activities. Therefore, only three scenarios are considered: a one-maneuver, two-maneuver, and three-maneuver control strategy. Based on a preliminary analysis, the most effective place to control the errors along the trajectory is periapsis; thus, the target location is limited to periapsis, reducing the design space even more. Given the constraint of not having maneuvers within a day of periapsis where most of the science activities take place, all subsequent maneuvers are placed exactly one day after the targeted periapsis. Recall that once the optimal target locations are identified, the maneuvers are moved around accordingly to minimize ΔV. Given all these assumptions and constraints, all possible target combinations are considered, i.e., 1-2-3, 1-2-4, ..., 20-21-22, and each combination is run in LAMBIC to collect maneuver and dispersion statistics. LAMBIC is a linear analysis of maneuvers with bounds and inequality constraints tool which produces the statistics of ΔV magnitude and delivery accuracy by simulating the execution of a sequence of maneuvers through a Monte Carlo process.[6] The simulation includes various sources of uncertainties including flyby error (dispersions after T126), orbit determination error, maneuver execution error (based on Cassini's most current Gates model), thruster firing control error (RCS effects), as well as uncertainty in Saturn's atmospheric model (drag effects).

Once the global search is performed, the output parameters taken into consideration are the total ΔV for either one, two, or three maneuvers ($1-\sigma$, μ, and $\Delta V99$ values), the average periapsis dispersions through 22 revs (1-σ values), and the number of periapsis out of bounds. To filter solutions out, a feasibility criteria is established as follows:

- average periapses dispersions $\leq$ 250 km
- total $\Delta V99 \leq 2$ m/s
- number of out-of-bound periapsis ≤ 5

The one-, two-, and three-maneuver strategies required 22, 231, and 1540 LAMBIC runs, respectively. The outcome of the simulation is to determine the optimal target location for each control strategy based on this linear brute force approach, and the filtered results, i.e., the solutions that meet the criteria listed above, are illustrated in Fig. 8. The optimal target location combination is identified from the lower left corner in each plot. For instance, consider the results from the one-maneuver control strategy global search. The dispersion-ΔV data point for each combination is represented by a blue dot and a number indicating the periapsis number targeting to. The optimal target location corresponds to the data point with lower average periapses dispersions (x-axis) and lower total $\Delta V99$ (y-axis), which for the one-maneuver strategy is the end of mission on 15-September-2017. This result is intuitive, i.e., if only one maneuver and one target are allowed, it makes most sense to place the burn at the beginning and target conditions at the end. However, the results from the two- and three-maneuver strategies are not as intuitive. Figures 8(b)-8(c) illustrate the rest of the results for the two- and three-maneuver cases, respectively. To avoid overcrowding the plots, the target combination labels are omitted. For the two-maneuver strategy, the optimal combination is periapsis-6 and periapsis-14, and for the three-maneuver strategy, the best location for the targets is at periapsis-6, periapsis-12, and periapsis-19 (as opposed to the intuitive choice of selecting periapsis-22 or the end of mission as the last target). The resulting trajectory dispersion plot for each strategy is shown in Fig. 9. Note that the peaks and troughs along these curves correspond to periapsis and apoapsis locations, respectively.

The optimal one-maneuver strategy result is unfavorable,

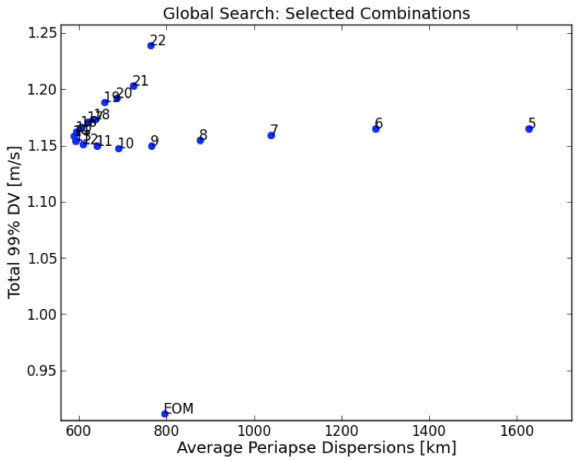

(a) Brute force results for the one-maneuver control strategy.

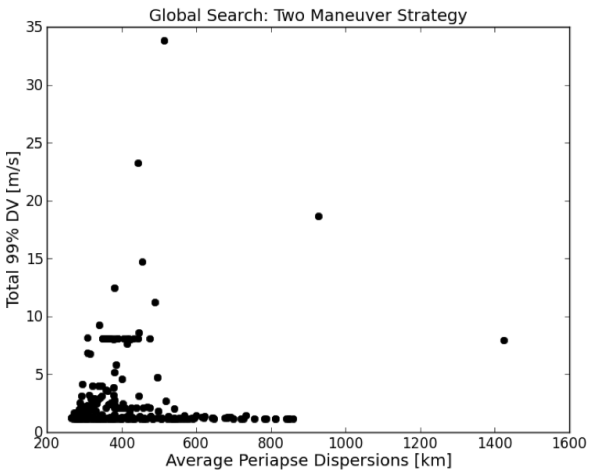

(b) Brute force results for the two-maneuver control strategy.

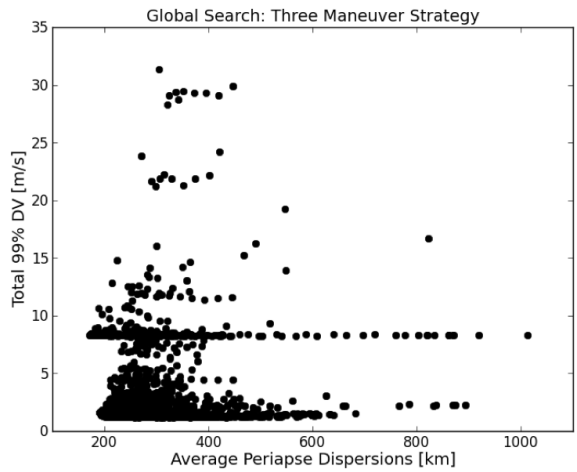

(c) Brute force results for the three-maneuver control strategy.

Fig. 8. Results from the global search for the target placement analysis.

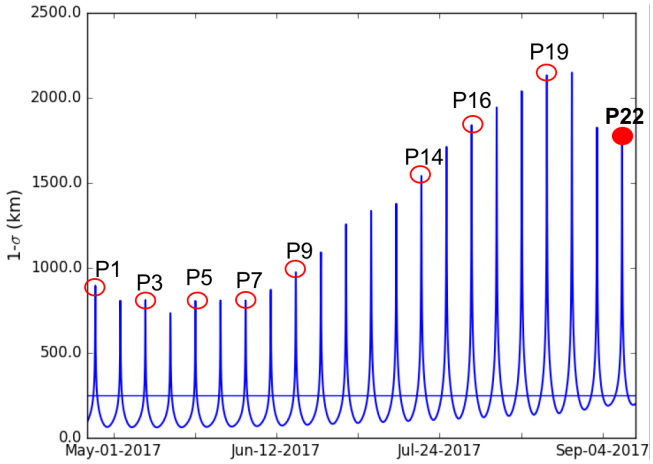

(a) Dispersions for one-maneuver control strategy targeting to P22.

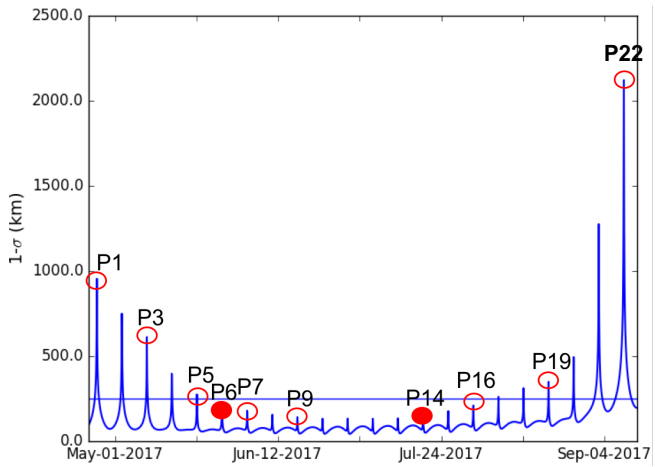

(b) Dispersions for two-maneuver control strategy targeting to P6 and P14.

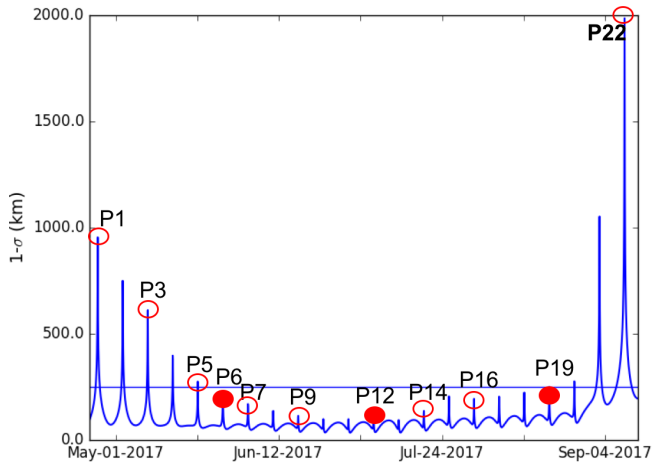

(c) Dispersions for three-maneuver control strategy targeting to P6, P12, P19.

Fig. 9. 1-σ Position uncertainties for each optimal target location run.

meaning that no periapsis is controlled within 250 km (1-σ) from the reference trajectory with one maneuver and one target only and, thus, it is discarded. Clearly, the more maneuvers, the lower the trajectory dispersions, that is, the dispersions are drastically reduced by adding a second maneuver (Fig. 9(a) vs. Fig. 9(b)). However, note that the first few periapses remain uncontrolled for the all depicted optimal control strategies. That is because controlling the first segment of the trajectory requires a large amount of ΔV – on the order of 25 m/s to 30 m/s – mostly due to the T126 flyby errors. By adding a third maneuver, the number of uncontrolled periapses at the end of the trajectory is reduced by half at little cost, making the three-maneuver control strategy the most favorable one.

2.3.2. Maneuver Placement Analysis

Once the target location is specified for each control strategy, the optimal location of the associated targeting maneuver

to minimize ΔV cost is also found linearly from STM elements. An effective and quick way of calculating the optimal maneuver location to target to the selected periapsis is to exploit the K-matrix, such that,

$$\Delta \mathbf{V} = K^{-1} \Delta \bar{\mathbf{X}}_f \tag{3}$$

where K is the upper right 3×3 block of the state transition matrix (ϕ), i.e.,

$$K = \begin{bmatrix} \phi_{14} & \phi_{15} & \phi_{16} \\ \phi_{24} & \phi_{25} & \phi_{26} \\ \phi_{34} & \phi_{35} & \phi_{36} \end{bmatrix} = \begin{bmatrix} \frac{\delta x_f}{\delta \dot{x}_0} & \frac{\delta x_f}{\delta \dot{y}_0} & \frac{\delta x_f}{\delta \dot{z}_0} \\ \frac{\delta y_f}{\delta \dot{x}_0} & \frac{\delta y_f}{\delta \dot{y}_0} & \frac{\delta y_f}{\delta \dot{z}_0} \\ \frac{\delta z_f}{\delta \dot{x}_0} & \frac{\delta z_f}{\delta \dot{y}_0} & \frac{\delta z_f}{\delta \dot{z}_0} \end{bmatrix} \tag{4}$$

and $\Delta \bar{\mathbf{X}}_f$ represents the changes, or corrections, to the final state. In essence, the minimum-ΔV location along a given orbit can be calculated by evaluating the norm of the inverse of the K-matrix. That is, when $\|K^{-1}\|$ is minimum, then the required ΔV is also minimum. Thus, given a fixed target downstream (periapsis-j), the selected orbit for maneuver placement (from periapsis-i to periapsis-i+1) can be split into a desired number of intervals and the corresponding ΔV value can be calculated using equation 3, as illustrated in Fig. 10. The STM components are evaluated at the selected one-hour time intervals (t_0 to t_f, t_1 to t_f, ..., t_{f-1} to t_f) over the length of the selected orbit (approximately 6.5 days long). Once the resulting ΔV values are collected, they are plotted as a function of time. Figure 11 illustrates a representative example associated with the three maneuver strategy: a maneuver is to be designed and placed between periapsis-6 and periapsis-7 with a fixed target at periapsis-12. The resulting curve figuratively represents the ΔV cost associated with placing the maneuver at any one-hour interval along the selected rev targeted to periapsis-12. Two minimum points on this curve, corresponding to minimum ΔV locations, are represented by blue dots and the associated epochs are labeled. These two minimums represent candidate locations to place the prime and backup maneuvers; however, the first local minimum violates the one-day constraint from periapsis, therefore, the prime maneuver is placed a few hours later at the 24 hr mark after the targeted periapsis at a small cost. The backup maneuver is then placed at the second minimum, allowing enough time between maneuvers at no cost. In fact, the backup occurs at more ΔV-efficient location than the prime. The specific ΔV cost in m/s is not given on the plot, but could be easily calculated using Equation 3.

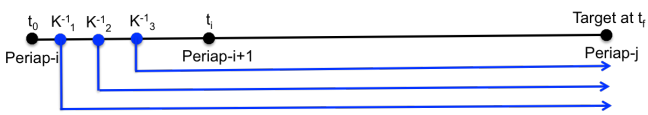

Fig. 10. Schematic to illustrate how the ΔV curve is generated: blue dots indicate locations along a given rev (from periapsis-i to periapsis-i+1) at which the norm of the inverse of the K-matrix is calculated based on the state transition matrix components ($\phi_{3\times3}(t_i, t_f)$)

Two noticeable peaks appear at two different locations on the curve in Fig. 11: one in between periapsis and apoapsis, and a second one right past apoapsis. Note that, although not clearly seen in Fig. 11, there are spikes that form right at periapsis-6

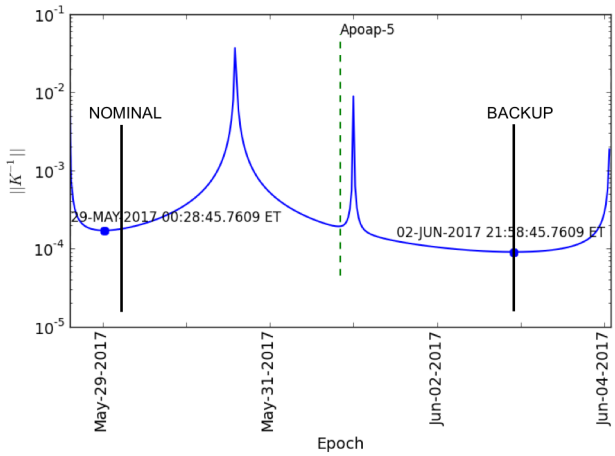

Fig. 11. Representative example illustrating the norm of the inverse of the K-matrix as a function of time: the minimum point on the curve represents the optimal location for maneuver placement between periapsis-6 and periapsis-7 with the target fixed at periapsis-12.

and periapsis-7. These spikes are expected to occur and correspond to a 180-degree transfer singularity. Similarly, because of the same geometry constraint, it is expected that a peak occurs at apoapsis; however, that is not the case. There is a peak forming *near* apoapsis. It is well-understood that there is an orbital transfer singularity due to a geometry constraint at periapsis and apoapsis (i.e., at 0, 180, and 360 degrees transfer angles). For these specific transfer angles, the Lambert problem faces a singularity. The plane of the orbit is defined by two position vectors (the space triangle). If the two position vectors are collinear with the central mass, then the plane is undefined and a singularity in the equation arises, resulting in a ΔV of infinite magnitude (theoretically). Therefore, one would expect a peak to appear right at apoapsis when the target is placed at a periapsis downstream (180 degrees apart). In an attempt to explain why the peak is slightly shifted from the expected apse location, a two-body analysis was performed. That is, all the additional gravitational bodies initially considered in the trajectory propagation model are removed as well as the gravity harmonics for Saturn. In essence, Saturn is treated as a point mass and no other bodies are perturbing the spacecraft trajectory. If the analysis is carried out in this simplified model, then the location of the first peak shifts to apoapsis, as one would expect (Fig. 12). Nevertheless, additional gravitational body effects and Saturn J2 terms cause the shift in the location of the first peak. Additionally, it is suspected that these extra terms have an effect on the maneuver size, i.e., they make the peaks on the ΔV curve more pronounced.

A similar plot is used to find an optimal placement for subsequent maneuvers, that is, for the second burn in the two-maneuver strategy, and the second and third burns in the three-maneuver strategy. After careful evaluation, it was determined that the three maneuver control strategy was better suited for this problem, even from a ΔV perspective: there are more periapses controlled under the 250 km position dispersion threshold and the $\Delta V99$ cost between the two- and three-maneuver cases was not large enough to disqualify the three-maneuver strategy. Eventually, the linear analysis resulted in the the optimal control strategy illustrated in Fig. 13: there are three maneuvers,

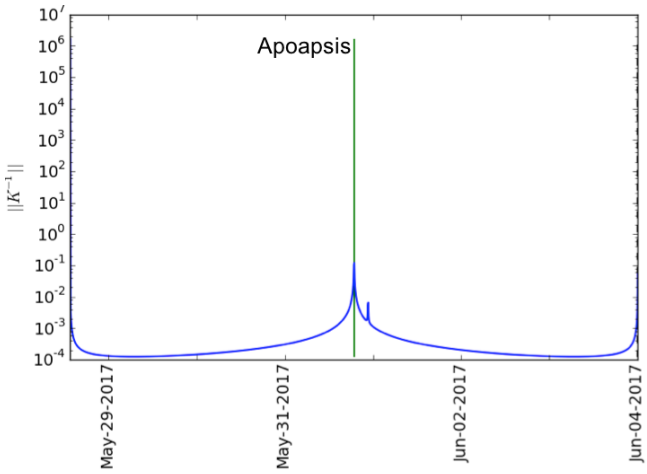

Fig. 12. Simplified two-body analysis: multi-rev targeting scenario, where the target is placed at any other periapsis downstream (at periapsis-12 in this illustrative example). By removing the J2 affects, the central peak shifts exactly to the apoapsis location.

Table 1. Statistical ΔV breakdown for the optimal control strategy resulting from the linear analysis detailed in Fig. 13.

ΔV	OTM470	OTM471	OTM472	Total
μ, m/s	0.353	0.032	0.008	0.394
1-σ, m/s	0.231	0.021	0.011	0.244
99%, m/s	1.119	0.092	0.058	1.193

OTM470 on 24-April-2017 shortly after the last targeted Titan flyby, T126, OTM471 on 29-May-2017 and lastly OTM472 on 07-July-2017 with corresponding targets on 28-May-2017, 06-July-2017 and 20-August-2017. The ΔV breakdown for each maneuver is detailed in Table 1.

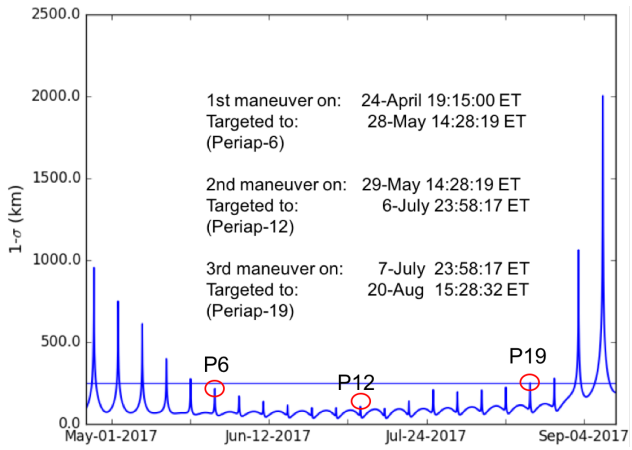

Fig. 13. Optimal control strategy resulting from the linear analysis: three maneuvers targeting to P6, P12, and P19, respectively.

2.4. The Actual Controlled Trajectory

The control strategy ultimately adopted by the Cassini Project and the trajectory dispersion results from the nonlinear approach were detailed in a paper by Wong et. al.[5] For reference, these results appear in Fig. 14(a) and the associated ΔV cost is detailed in Table 2. For reasons related to science observations and sensitivities to timing errors, the Cassini Project decided that there were only three periapses that needed to be controlled and maintained under 250 km at the 68th percentile, as opposed to attempting to maintain the entire trajectory under this control. Specifically, these control points are periapsis-3 (P3) on 09-May-2017, periapsis-13 (P13) on 12-July-2017, and periapsis-16 (P16) on 01-Aug-2017. The first maneuver, OTM470, is left at the same location; OTM471 occurs on 10-May-2017 and OTM472 is scheduled for 15-July-2017.

Table 2. Statistical ΔV breakdown for the selected control strategy based on Project decision (based on linear approach).

ΔV	OTM470	OTM471	OTM472	Total
μ, m/s	0.450	0.108	0.057	0.615
1-σ, m/s	0.274	0.070	0.041	0.341
99%, m/s	1.267	0.320	0.181	1.670

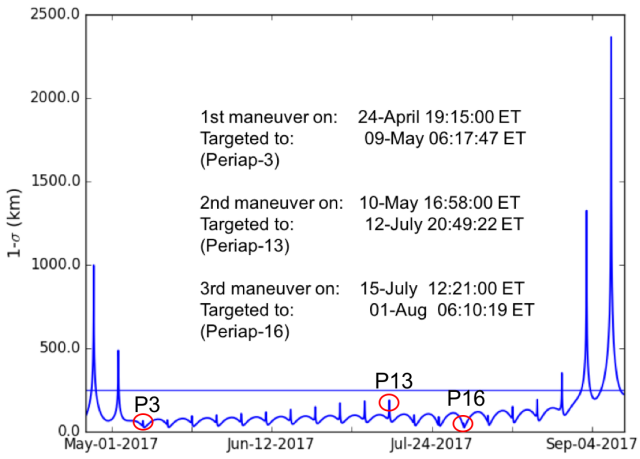

(a) Trajectory dispersions for the selected three-maneuver control targeting to periapsis-3, periapsis-13 and periapsis-16 based on the linear approach.

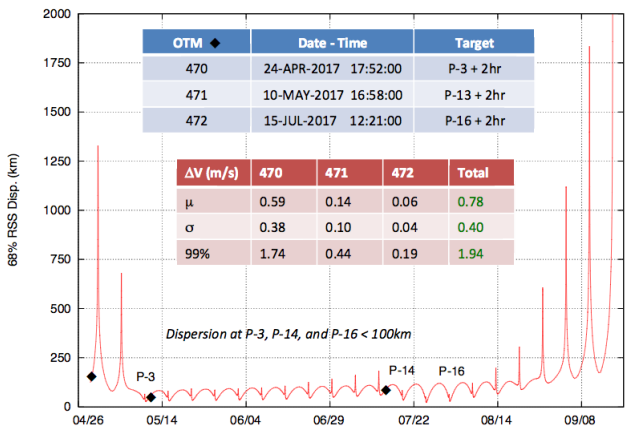

(b) Trajectory dispersions for the selected three-maneuver control targeting to periapsis-3, periapsis-13 and periapsis-16 based on the nonlinear approach[5] (given for comparison and validation purposes with Fig. 14(a)).

Fig. 14. Linear vs. nonlinear dispersion results for the selected three-maneuver control strategy by the Cassini Project.

By moving the first target to an earlier time, the position dispersion decreases significantly from over 1300 km at P1 to approximately 60 km at P3, at the expense of increasing the $\Delta V99$ cost from 0.35 m/s to 0.42 m/s. This increase is not insignificant given the small amount of propellant left in the tanks. Additionally, by moving the last target to an earlier epoch, the position dispersion at the subsequent six periapses increases significantly. Nevertheless, this turned out to not be an issue since there are no time-error sensitive science observations planned during those trajectory segments. In the end, the Cassini Navigation team designed a suitable control strategy using only three

OTMs with a $\Delta V99$ usage of less than 2 m/s to adequately control the trajectory while meeting science planning requirements and requests.

2.5. Remarks: Linear vs. Nonlinear Analysis

There are fundamental differences between a linear and nonlinear analysis of dynamical systems. The linear approach employed in this investigation relies on covariance mapping based on the unperturbed reference trajectory. As so, it is applicable to this particular problem as long as its validity is established by comparing the linear results to the results from a full, nonlinear analysis. The linear assumptions of small deviations and the independence of contributions from various error sources are not necessarily apparent for certain problems, including this one.

In this investigation, a self-consistent numerical model that closely simulated the underlying physics of the problem was readily available to accurately model and statistically analyze the trajectory. Consequently, it was straightforward to validate the results from the linear approach, allowing the analysts to fully exploit the benefits of a linear simulation to solve this problem, more specifically, the short computational time aspect. That is, it was possible to quickly find an optimal trajectory control strategy without the need to use long numerical propagations or complex optimization schemes.

The intent of this paper is not to emphasize a set of specific results particular to the Cassini Grand Finale Mission, but rather to highlight the benefits of applying a linear approach early on in the design process. More often than not, analysts seek the truth, or accurate answers, by relying on highly complex numerical schemes and optimization method, but sometimes the simpler methods offer great insight into the design space at little cost, and the problem detailed in this paper is a great example of such.

3. Acknowledgements

This research was carried out at the Jet Propulsion Laboratory, California Institute of Technology, under a contract with the National Aeronautics and Space Administration. © 2017 California Institute of Technology. Government sponsorship acknowledged.

References

1) Roth, D., e. a., Cassini Tour Navigation Strategy, *AAS/AIAA Astrodynamics Specialist Conference*, AAS Paper 03-546, Big Sky, Montana, August 3-7 2003.
2) Smith, J. and Buffington, B., Overview of the Cassini Solstice Mission Trajectory, *AAS/AIAA Astrodynamics Specialist Conference*, AAS Paper 09-351, Pittsburgh, PA, August 9-13, 2009.
3) Buffington, B., Strange, N., and Smith, J., Overview of the Cassini Extended Mission Trajectory, *AIAA/AAS Astrodynamics Specialist Conference*, AIAA-2008-6752, Honolulu, Hawaii, August 18-21, 2008.
4) Buffington B., Smith J., Petropoulos A., Pelletier F., and Jones J., Proposed End-Of-Mission for the Cassini Spacecraft: Inner D Ring Ballistic Saturn Impact, *61st International Astronautical Congress*, Prague, CZ, September 27-October 1, 2010.
5) Wong, M., Hahn, Y., Roth, D. and Vaquero, M.,Trajectory Dispersion Control for the Cassini Grand Finale, *25th International Symposium on Space Flight Dynamics*, October 19-23, 2016, Munich, Germany.
6) Maize, E. H., Linear Statistical Analysis of Maneuver Optimization Strategies, *AAS/AIAA Astrodynamics Conference*, AAS Paper 87-486, Kalispell, Montana, August 10-13, 1987.